# Design Optimization for Low Voltage DC-DC Converter with Coupled Inductor Topology

Basavaraj V. Madiggond [1] H. N. Nagaraja [2]

**Abstract–Multiphase Synchronous Buck Converters also known as voltage regulator modules (VRMs) for microprocessor power delivery with coupled inductors at output are discussed. For feasible and effective ripple reduction, strong coupling is needed if the correct magnetic topology is used. For more than two phases, this can be a "ladder" core with windings around each rung. Typical ripple reduction is better than a factor of six with no effect on response time. One can also chose to improve response time while still significantly reducing ripple.**

**Key Words–Synchronous Buck Converter, Multiphase, Transient response, Coupled Inductor, Coupling coefficient.**

## I. INTRODUCTION

It is predicted that the future microprocessors demand more and more power and at the same time the required voltage levels continue to drop. In future voltage go below 1V and current will go beyond 100A [1]. To handle this huge current multiphase interleaving technology is preferred. The multiphase interleaving technology helps to reduce the current ripples at the output and improves the transient response [2]-[4]. The challenge is that the load current can change from near zero to full load or vice versa in nanoseconds and the voltage has to be maintained constant throughout. The combination of high current and fast response requires a voltage regulator module (VRM) located immediately adjacent to the load. The VRM must be small in size as well as have high efficiency and extremely fast response.

At present, the standard design used for high-performance VRMs is a buck converter with multiple parallel sections, staggered in phase [5], [6], In a buck converter with a load-current step, the output capacitor supplies (or sinks) the immediate difference in current while the inductor current is ramped up or down to match the new load current. A small inductor allows ramping the current quickly to minimize the output capacitor requirement. However, small inductor values also lead to large ripple current. In a single-phase converter, large ripple current in the inductor increases the output capacitor requirement when the inductor is very small [6]. The standard multiphase interleaved design avoids this problem because it achieves substantial ripple current cancellationin the output capacitor [7]. This allows smaller inductance without requiring a large output capacitor. However, the full ripple current flows through the MOSFET switches (including synchronous rectifiers) and through the inductor itself, resulting in higher losses and higher peak current requirements. One strategy to reduce the ripple current throughout is to operate at very high switching frequencies (e.g., see [6]), but this increases switching and gate-drive losses and imposes difficult requirements for magnetic materials capable of low loss at very high frequencies.

In [8], [9], it was shown that coupling the inductors in a two-phase interleaved converter can effect a reduction in ripple. Unlike the ripple cancellation in an uncoupled multiphase converter, this ripple reduction extends to the current in the inductor windings and in the switches. In [10], one topology for coupling larger numbers of inductors in a multiphase VRM is considered, but is not found to offer major advantages. In [11], design optimization of the coupled inductor is considered. However, the method employed there does not provide any insight regarding the influence of the design parameters on the losses and the performance of the converter.

In this paper, a novel coupled core structure along with a new method for estimating the losses and efficiency is proposed. The proposed core structure is shown in Fig. 1. It has a central leg called the leakage leg, surrounded by '*n*' number of side legs. The central leg has an adjustable air gap. By adjusting the length of the air gap the coupling coefficient can be varied. As the central leg is equidistant from the surrounding legs, the reluctance offered to individual phase flux are identical.

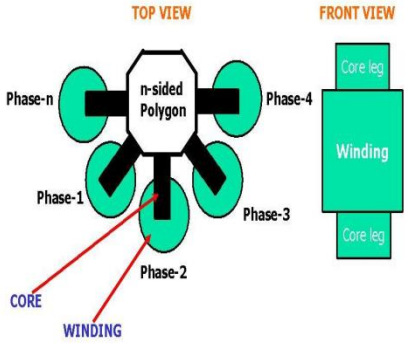


Fig. 1: Proposed coupled multiphase buck converter structure

## II. ANALYSIS OF THE UNCOUPLED INDUCTOR BUCK CONVERTER

There are three main limitations of the single-phase buck regulator if employed in a voltage regulator for desktop, notebook or server applications. First, the high currents — greater than 40 A for notebook, 120 A for desktop and 150 A for server — would cause excessive $I^2R$ losses if delivered over one path or phase. Second, processors require low-output ripple voltage and this necessitates keeping the output ripple current low, as $V_{RIPPLE} = I_{RIPPLE}$ ESR. This implies the need for a large inductor because $I_{RIPPLE}$ is proportional to 1/L.

The paper first received 21 Jun. 2014 and in revised form 23 Dec 2014.
Digital Ref: APEJ-2014-06-0443

[1] **Jain College of Engineering, Belgaum, Karnataka, India, E-mail: basavarajvma@gmail.com**
[2] **Dean (Academics), Indus University Ahmedabad, Gujarat, India**

Third, the processor power supply must be able to respond quickly to changes in power requirements. Unfortunately, the third requirement, fast transient response, implies the need for a small inductor to allow the current through the supply to change quickly, and this conflicts directly with the need for a larger inductor to minimize output voltage ripple.

The uncoupled multiphase buck regulator was designed to resolve these three limitations. Instead of using a single high-current path, the multiphase buck breaks the current into several lower current parallel paths or phases. Each phase has its own inductor and set of switches, and the current in each phase is summed to form the output current. By activating each phase at a different point in the cycle, the ripple currents of each phase can be overlapped to reduce the overall output current ripple. To simplify the analysis, a two-phase uncoupled buck with 180 degrees between phases will be discussed here. However, the same approach can be used with any number of phases operating at any phase angle.

A simplified schematic of a two-phase buck is shown in Fig. 2. A two-phase buck has four states of operation. During the first state, the input voltage is connected to phase one, and energy is both being transferred to the output and stored in the inductor L1. At the same time, the input side of phase two is connected to ground and the inductor L2 transfers energy to the output. During the second state, the input sides of both phases are connected to ground and both inductors (L1 and L2) transfer energy to the output. This cycle is repeated over states three and four, the only difference being that phase two is connected to the input while phase one is connected to ground, and then both phases are connected to ground.

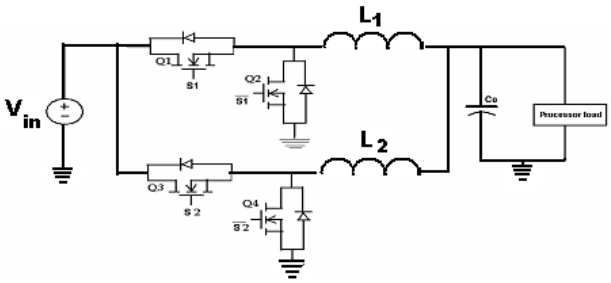


Fig. 2: Uncoupled Two phase synchronous buck converter

## III. Analysis of the Coupled Inductor Buck Converter

In the proposed core structure, any number of phases can be coupled. Fig. 3(a) shows the general schematic diagram of an *n* phase coupled buck converter. Under the assumptions of identical phases and ideal switches, the equivalent representation of an *n* phase coupled buck converter is shown in Fig. 3(b).

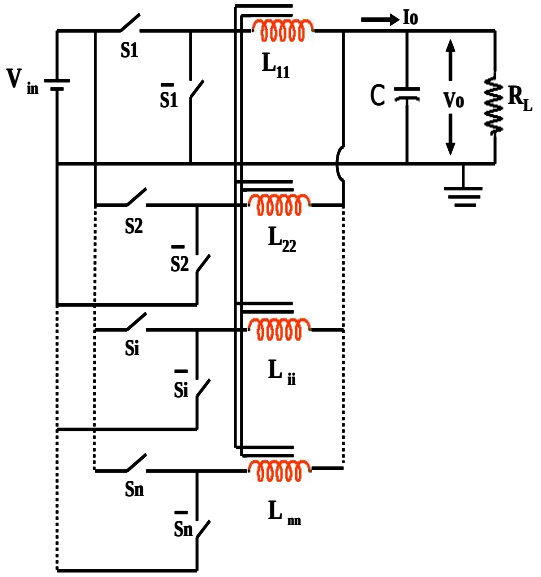


Fig. 3(a): General schematic diagram of an n phase coupled buck converter

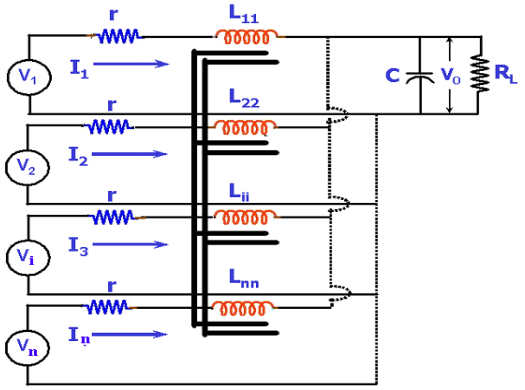


Fig. 3 (b): Coupled multiphase buck converter with filter inductor in each phase

where,

$$V_i = V_{in}.S_i \qquad (1)$$

$$S_i = 1 \; ; \quad for \; \frac{(i-1)}{n}.T \le t \le \frac{(i-1)}{n}.T + T_{on}$$
$$= 0;$$

Otherwise

$$T_{on} = D.T$$

where,
'*D*' is the duty cycle; *T* is the switching period; and '*n'* is the number of phases. It was shown in [12] that, such a coupled buck converter can be represented by one common mode and (*n-1*) differential mode equivalent circuits provided the self and mutual inductances of all the phases are identical. These equivalent circuits are shown in Fig. 4(a) and 4(b).

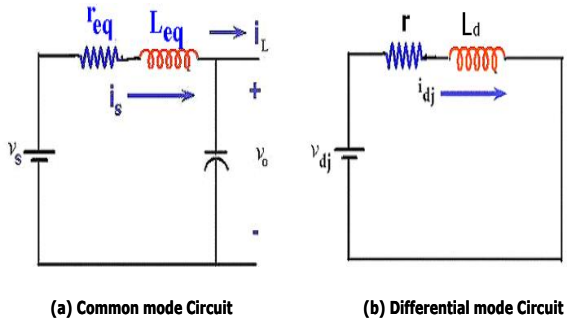


Fig. 4. Coupled converter equivalent circuits

where,

$V_s \triangleq \frac{1}{n}\sum_{i=1}^{n} Vi$ ; $i_s \triangleq \sum_{i=1}^{n} ii$ ; $r_{eq} \triangleq \frac{r}{n}$

$$Leq \triangleq \frac{Ls}{n} = \frac{L - \sum_{i=1}^{n-1} Mi}{n}$$

For $2 \le j \le n$

$V_{dj} \triangleq V_{j-1} - V_j = r i_{dj} + L_d \, p \, i_{dj}$ ;

$I_{dj} \triangleq i_{j-1} - i_j$ ;

$L_d = (L+M) \, . \, I_{(n-1).(n-1)}$

## IV. COUPLED CORE DESIGN OF MULTIPHASE BUCK CONVERTER

The coupled inductor concept and its advantages may be extended to any number of phases. For simplicity, we have taken a four-phase coupled structure, maintaining the shape of the core to be the same. The four coils are connected in the four legs of the new core structure. It should be noted that, due to the structural symmetry of the proposed core, the assumptions made for deriving the common mode and differential mode equivalent circuits will be satisfied.

During the steady state, a part of the flux produced by the inductor currents passes through the center leg. The center leg has an air gap, whose length can be adjusted for achieving a better coupling coefficient. Higher the coupling, greater is the ripple reduction. Even the transient response has found to be improved by experiment. In the phase legs, the flux produced by one coil opposes the other. In the new proposed core structure, our intention is to draw less Ampere turn from the source and meet the requirement. Here, the intention is to avoid saturation of the core and as far as possible use all the windings equally. Fig. 5 shows the electrical equivalent model of the multiphase coupled core structure shown in Fig. 1.

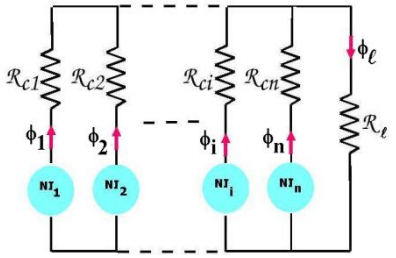


Fig.5. Electrical Equivalent model for multiphase coupled core structure R c and Rl are the core and leakage path reluctance respectively.

The equivalent reluctance as seen by each MMF source of the model shown in Fig. 5 is

$$\mathcal{R}_{eq} = \mathcal{R}_c + \frac{\frac{\mathcal{R}_c}{n-1}.\mathcal{R}_f}{\frac{\mathcal{R}_c}{n-1} + \mathcal{R}_f} \qquad (2)$$

Where, $\mathcal{R}_c$ is the reluctance of each core leg and $\mathcal{R}_f$ is the reluctance of the central leakage path.

$$\therefore \mathcal{R}_{eq} = \mathcal{R}_c \cdot \frac{1 + n.k_r}{1 + (n-1).k_r} \quad ;$$

$$\text{where } k_r = \frac{\mathcal{R}_f}{\mathcal{R}_c} \qquad (3)$$

The self and mutual inductances of the coupled inductor are

$$L = \frac{N_c^2}{\mathcal{R}_{eq}} = \frac{N_c^2}{\mathcal{R}_c} \frac{1 + (n-1).k_r}{1 + n.k_r} \quad ; \qquad (4)$$

$n$ = number of phases; $N_c$ is the number of turns in each phase leg

$$M = \frac{N_c^2}{\mathcal{R}_c} \times \frac{k_r}{1 + n.k_r} \qquad (5)$$

The common mode and the differential mode inductances are given by

$$L_{eq} \triangleq \frac{Ls}{n} = \frac{L-(n-1)M}{n} = \frac{Nc2}{nRc} \cdot \frac{1}{1+nkr}$$

$$L_d = L + M = \frac{N_c^2}{\mathcal{R}_c} \qquad (6)$$

Using the model shown in Fig. 5, we intend to calculate the magnetic flux waveform which has both dc and ac components. The dc components are calculated by assuming that the dc currents in each phase are equal. Thus, for '$n$' phases connected in parallel, the dc component of phase current is given by $\frac{I_S}{n}$.

Flux in the core phase legs:

With reference to the Fig. 5, flux in each phase leg is given by

$$\phi_i = \phi_{ii} - \sum_{\substack{j=1 \\ i \neq j}}^{n} \phi_{Mj} \tag{7}$$

where, $\phi_{ii}$ is the total flux produced in the leg i, $\phi_{Mj}$ is the mutual flux due to the $j^{th}$ coil.

$$\phi_i = \frac{1}{N_C}\left[ L.i_i - M\sum_{\substack{j=1 \\ j \neq i}}^{n} ij \right] = \frac{1}{N_C}\left[ (L+M).i_i - M.i_S \right] \tag{8}$$

$$\phi_i = \frac{N_c}{\mathcal{R}_c}[i_i - \frac{k_r}{1+n\cdot k_r}\cdot i_S] \tag{9}$$

$\therefore$ Peak value of

$$\phi_i = \phi_i = L_d.\hat{I}_{pc} - M.\hat{I}_s$$

Now,

$$\frac{\Delta I_{pc}}{I_{pc}} = \left[1 + \frac{(n-1)}{(1-n.D)}.\frac{L_s}{L_d}\right].\frac{\Delta I_s}{I_s}$$

$$\therefore \hat{\phi}_i = \frac{N_c I_s}{\mathcal{R}_c}[\frac{(1-n\cdot D)+\frac{1}{2}.n.(1-D)\frac{\Delta I_s}{I_s}}{n.(1+n\cdot k_r)(1-n\cdot D)}]$$

Peak flux density in the core legs is given by

$$\hat{B}_i = \frac{\hat{\phi}_i}{A_c} \tag{10}$$

where, $A_c$ is the phase leg cross sectional area Flux in the leakage path (central leg)

From Fig. 5

$$\phi_l = \frac{\frac{\mathcal{R}_c}{(n-1)}}{\frac{\mathcal{R}_c}{(n-1)} + \mathcal{R}_l}.\sum_{i=1}^{j}\phi_{ii} \tag{11}$$

$$OR \quad \phi_l = \frac{\mathcal{R}_c}{\mathcal{R}_c + (n-1).\mathcal{R}_l}\cdot\frac{N_c\cdot I_s}{\mathcal{R}_{eq}}$$

$\therefore$ Peak value of $\phi_l$ is given by

$$\hat{\phi}_l = \frac{N_c I_s}{(1+n.k_r)\cdot\mathcal{R}_c}[\frac{1}{n} + \frac{1-D}{1-n.D}\cdot\frac{1}{2}\cdot\frac{\Delta I_s}{I_s}] \tag{12}$$

$\therefore$ Peak flux density in the leakage path is

$$\hat{B}_l = \frac{\hat{\phi}_l}{A_l} \tag{13}$$

where $A_l$ is the central leg cross sectional area Ac flux in the core legs

$$\Delta\phi_i = \frac{(1-D).N_c\cdot\Delta I_s}{(1-n.D).(1+n.\ k_r)\cdot\mathcal{R}_c} \tag{14}$$

$$\Delta B_i = \frac{\Delta\phi_i}{A_c} \tag{15}$$

Ac flux in the leakage path

$$\Delta\phi_l = \frac{N_c\cdot\Delta I_s}{(1+n.\ k_r)\cdot\mathcal{R}_c} \tag{16}$$

$$\Delta B_l = \frac{\Delta\phi_l}{A_l} \tag{17}$$

1). Loss estimation in the Coupled Converter

Fig. 6 shows the cross sectional diagram of coupled core structure

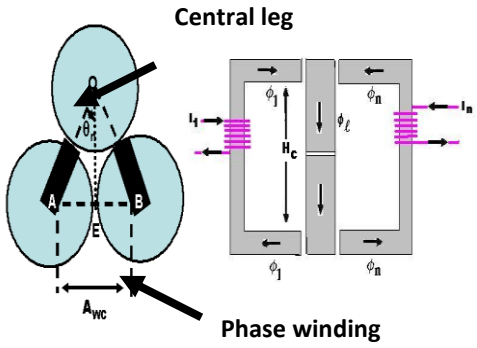


Fig. 6. Cross sectional view of the coupled core structure

With reference to Fig. 6,

$\frac{A_{WC}}{2}$ =Window area,

$A_c$ =Core area, $H_c$ =Window height

Volume of outer legs:

Length of each outer leg =

$$(H_c + \sqrt{A_c}) + 2.[\frac{A_{wc} + \sqrt{A_c}.H_c}{2.H_c.\sin\theta_n} - \sqrt{\frac{A_l}{\pi}}] \tag{18}$$

Total volume of the core with '*n*' legs

$$= \frac{n.A_c.H_c}{\sin\theta_n}.[\sin\theta_n + \frac{\sqrt{A_c}}{H_c}.\left\{1 + \sin\theta_n(1 - \frac{2}{\sqrt{\pi}}\sqrt{\frac{A_l}{A_C}}\right\} + \frac{A_{WC}}{H_c^2}] \tag{19}$$

Assuming the core loss to be $W_i$ / unit volume at $\Delta B = B_{max}$ and $f = f_{sw}$

Core loss in the outer phase legs is= $W_i\cdot(\frac{\Delta B_i}{B_{max}})^2$ * Total volume of phase legs

$$= W_i\cdot\left(\frac{\Delta I_s.N_c}{A_c.\mathcal{R}_c.B_{max}}\right)^2\cdot\frac{(1-D)^2}{(1-n.D)^2.(1+n.k_r)^2}$$

$$*[\frac{n.A_c.H_c}{\sin\theta_n}\left\{\sin\theta_n + \frac{\sqrt{A_c}}{H_c}(1+\sin\theta_n - \frac{2}{\sqrt{\pi}}.\sqrt{\frac{A_l}{A_c}}.\sin\theta_n) + \frac{A_{WC}}{H_c^2}\right\} \tag{20}$$

Volume of leakage path

$$= (H_c + \sqrt{A_c}).A_l \quad (21)$$

Core loss in leakage path = $n.W_i.(\frac{\Delta B_l}{B_{max}})^2$ *

Volume of the leakage path =

$$W_i.\left(\frac{\Delta I_s.N_c}{A_c.\mathcal{R}_c.B_{max}}\right)^2.\frac{n}{(1+n.k_r)^2}.\left(\frac{A_c}{A_l}\right)^2.[H_c.A_c(1+\frac{\sqrt{A_c}}{H_c}).\frac{A_l}{A_c}] \quad (22)$$

Therefore total losses in the coupled core can be expressed as

$$W_{ic} = n.W_i.H_c.A_c.\left(\frac{\Delta I_s.N_c}{A_c.\mathcal{R}_c.B_{max}}\right)^2.\frac{1}{(1+n.k_r)^2}[\frac{(1-D)^2}{(1-n.D)^2.\sin\theta_n} * \left\{\sin\theta_n + \frac{\sqrt{A_c}}{H_c}(1+\sin\theta_n - \frac{2}{\sqrt{\pi}}.\sqrt{\frac{A_l}{A_c}}.\sin\theta_n) + \frac{A_{wc}}{H_c^2}\right\} + .(1+\frac{\sqrt{A_c}}{H_c}).\frac{A_c}{A_l}] \quad (23)$$

Losses in the MOSFETS:

Assuming the $R_{DS\text{-}ON}$ of the high side and low side MOSFETS to be the same, the losses during steady state is given by,

$$W_{MOSFET} = n * I_{RMS}^2 * R_{DS\text{-}ON};$$

where, $I_{RMS} = \frac{I_s}{n} * (1 + \frac{K_C^2}{12})^{\frac{1}{2}}$

$$W_{MOSFET} = \frac{I_s^2}{n} * (1 + \frac{K_C^2}{12}).R_{DS-ON} \quad (24)$$

where, $K_C = \left[\frac{n*[(1-D)+K*(1-n.D)]}{(1-n.D)*(1+n.K)}\right].\frac{\Delta I_s}{I_s}$

$K = \frac{M}{L} = \frac{k_r}{1+(n-1).k_r}$ = Coupling coefficient;

$D$ = Duty ratio

Loss in the Inductor due to ESR:

$W_{L\,(ESR)} = I^2_{RMS} * ESR_L$

$ESR_L$ is given by $[\frac{\pi.\rho.N_c^2}{H_c} + \frac{\pi.\rho.N_c.\sqrt{A_c}}{C_w}]$

where ρ is the specific resistance of the winding material, $C_w$ is the winding cross sectional area.

$$W_{L(ESR)} = \frac{I_s^2}{n^2} * (1 + \frac{K_C^2}{12}) [\frac{\pi.\rho.N_c^2}{H_c} + \frac{\pi.\rho.N_c.\sqrt{A_c}}{C_w}] \quad (25)$$

Therefore, total loss in the coupled core topology is given by,

$W_{total} = W_{ic} + W_{MOSFET} + W_{L\,(ESR)}$

$$W_{total} = n.W_i.H_c.A_c.\left(\frac{\Delta I_0.N_c}{A_c.\mathcal{R}_c.B_{max}}\right)^2.\frac{1}{(1+k_r)^2}[\frac{(1-D)^2}{(1-n.D)^2.\sin\theta_n} * \left\{\sin\theta_n + \frac{\sqrt{A_c}}{H_c} * (1+\sin\theta_n - \frac{2}{\sqrt{\pi}}.\sqrt{\frac{A_l}{A_c}}.\sin\theta_n) + \frac{A_{wc}}{H_c^2}\right\} + (1+\frac{\sqrt{A_c}}{H_c}).\frac{A_c}{A_l}] + \frac{I_0^2}{n}(1+\frac{K_c^2}{12}) * [R_{DS-ON} + \{\frac{\pi.\rho.N_c^2}{H_c} + \frac{\pi.\rho.N_c.\sqrt{A_c}}{C_w}\}] \quad (26)$$

2). Loss estimation in uncoupled case

Fig. 7 shows the cross sectional view of the uncoupled core structure.

*The maximum ac flux flowing in the core* is given by

$$\hat{\phi}_{max} = \frac{N_u.I_s}{\mathcal{R}_u}[\frac{1}{n} + \frac{\Delta I_s}{2.I_s}.\frac{(1-D)}{(1-n.D)}] \quad (27)$$

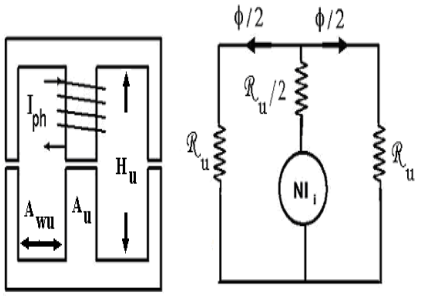


Fig. 7: Uncoupled core structure with its equivalent model

where, $I_O$ is the output load current, $D$ is the duty cycle and $N_u$ is the number of turns in the winding.

Ac flux in the core, is given by

$$\Delta\phi_i = \frac{N_u.\Delta I_O}{\mathcal{R}_u}\frac{(1-D)}{(1-n.D)} \quad (28)$$

Total core loss in the uncoupled core is given by

$$W_{iu} = W_i.\left(\frac{\frac{\Delta\phi_t}{A_u}}{\frac{\hat{\phi}_{Max}}{A_u}}\right)^2 * \text{Volume of the core}$$

$A_u$ is the core cross sectional area, $\mathcal{R}_u$ is the reluctance of the core leg

$$W_{iu} = W_i.\left(\frac{N_u.\Delta I_0}{A_u.\mathcal{R}_u.B_{max}}\right)^2.\frac{(1-D)^2}{(1-n.D)^2}.[n.\frac{A_u}{H_u}(2.H_u^2 + 2.A_{wu} + 2.H_u.\sqrt{A_u})] \quad (29)$$

Loss in the Inductor due to ESR:

$W_{L\,(ESR)} = I^2_{RMS} * ESR_L$

$$W_{L(ESR)} = \frac{I_O^2}{n^2} * (1 + \frac{K_U^2}{12}) \left[\frac{\pi.\rho.N_U^2}{H_U} + \frac{\pi.\rho.N_U.\sqrt{A_U}}{C_w}\right] \quad (30)$$

where, $K_U = \frac{n.(1-D)}{(1-n.D)}$

Loss in the MOSFET due to $R_{DS\text{-}ON}$

$$W_{MOSFET} = \frac{I_O^2}{n} * (1 + \frac{K_U^2}{12}).R_{DS-ON} \quad (31)$$

$\therefore$ Total loss in the uncoupled circuit is

$$W_{u\text{-}total} = n.W_i.H_u.A_u.\left(\frac{N_u.\Delta I_0}{A_u.\mathcal{R}_u.B_{max}}\right)^2.\frac{(1-D)^2}{(1-n.D)^2}.(2+2.\frac{A_{wu}}{H_u^2}+2.\frac{\sqrt{A_u}}{H_u}) + \frac{I_0^2}{n.(1-D)}(1-D+2.K_u.D-2.D^2.K_u+D^2.K_u^2-\frac{D}{12}.K_u^2+\frac{K_u^2}{12})* (\pi.\rho.\frac{N_u^2}{H_u}+\pi.\rho.\frac{N_u.\sqrt{A_u}}{C_w}+R_{DS\text{-}ON}) \quad (32)$$

LOSS FUNCTION = *Ratio of coupled to uncoupled total losses* (Eqn. 26 and 32)

$\therefore$ LOSS FUNCTION

$$= \frac{W_{ic} + W_{L(ESR)} + W_{MOSFET}}{W_{iu} + W_{L(ESR)} + W_{MOSFET}}$$

After taking the ratio of total losses between coupled and uncoupled converters, we have further expressed the coupled terms in terms of uncoupled parameters, so as to get all unknown coupled variables in terms of known uncoupled variables with valid assumptions.

## V. Optimization of Loss Function

In order to estimate the efficiency improvement and to predict the losses in the coupled system, a comparative analysis between uncoupled and coupled is made by taking the ratios of many variable parameters viz.,

$X = \frac{A_{wu}}{A_u}$ = Ratio of window to core area in uncoupled case equal to 1.5 (assumed)

$X1 = \frac{A_c}{A_u}$ = Ratio of coupled to uncoupled core cross sectional areas

$X2 = \frac{N_c}{N_u}$ = Ratio of coupled to uncoupled number of turns.

$X3 = \frac{A_{wc}}{A_c}$ = Ratio of window to core cross sectional area in the coupled converter

$X4 = \frac{l_l}{l_c}$ = Ratio of leakage air gap length to core air gap length in coupled core

$X5 = \frac{A_c}{A_l}$ = Ratio of core to leakage path cross sectional area in coupled converter

$X6 = \frac{H_c}{H_u}$ =1 (assumed)

The basis of comparison are $I_s=I_o$, $L_s = \frac{L_u}{n}$; where $L_u$ is the self-inductance of the coil $L_s$ is the equivalent inductance

1). Constraint equations:

The loss function to be optimized has the numerator and denominator terms in the six variables mentioned above. We have used Lagrange's method of optimization. The constraint equations we have considered are as follows:

a) Equality constraint equations:-

- *Foot print area ratio is equal to 1*

$$1.046 * X_1^2 * X_3^2 + 4.58 * X_1 + 4.71 * X_2^2 + 4.37 * X_1^{\frac{3}{2}} * X_3 + 9.28 * X_1^{\frac{1}{2}} * X_2 + 4.435 * X_1 * X_2 * X_3 - 61.4 = 0$$

- *Equivalent coupled inductance is 1/n times the equivalent uncoupled inductance.*

$$X_1 * X_2^2 - 4 * X_4 * X_5 - 1 = 0$$

b) Inequality constraint equations:-

- *Window area per turn in coupled case is greater than or equal to that of uncoupled case*

$$X_1.X_3 - 3.X_2 \geq 0$$

- *The weight of the coupled system must be less than or equal to the weight of the Uncoupled system*

$$24 * X_1 + 47.33 * X_1^{\frac{3}{2}} - 44.35 * X_1^{\frac{3}{2}} / sqrt(2 * X_1 * X_2^2 - 1) + 22.64 * X_1^2 * X_3 + 23.77 * X_1 / (2 * X_1 * X_2^2 - 1) + 19.4 * X_1^{\frac{3}{2}} / (2 * X_1 * X_2^2 - 1) + 56.08 * X_1^{\frac{3}{2}} + 22.9 * X_1^2 * X_3^2 \leq 509.72$$

- *Leakage leg area must be less than or equal to the difference of foot print area and the sum of core and winding area.*

$$\frac{4}{2.X_1.X_2^2 - 1} - 1.04 * X_1.X_3^2 + 14.14.\frac{X_2^2}{X_1} - 4.37 * \sqrt{X_1}.X_3 + 21.5.\frac{X_2}{\sqrt{X_1}} - 4.44.X_2.X_3 + 8 \leq 0$$

**Table 1:Loss estimation in coupled core with variation of foot print area ratio**

| Variables | FPA ratio at weight ratio=1 | | | | | | | | | |
|---|---|---|---|---|---|---|---|---|---|---|
| | **0.6** | **0.7** | **0.8** | **0.9** | **1.0** | **1.1** | **1.2** | **1.3** | **1.4** | **1.5** |
| **$X_1$** | 2.51 | 3.037 | 3.19 | 3.335 | 3.47 | 3.6 | 3.73 | 3.85 | 3.96 | 4.07 |
| **$X_2$** | 0.51 | 0.465 | 0.45 | 0.434 | 0.42 | 0.41 | 0.40 | 0.395 | 0.388 | 0.38 |
| **$X_3$** | 0.61 | 0.586 | 0.68 | 0.758 | 0.83 | 0.88 | 0.94 | 0.987 | 1.03 | 1.07 |
| **Loss ratio** | 0.91 | 0.907 | 0.905 | 0.902 | 0.9 | 0.899 | 0.898 | 0.897 | 0.896 | 0.89 |

$$X_1 = \frac{A_C}{A_U};\ X_2 = \frac{N_2}{N_1};\ X_3 = \frac{A_{WC}}{A_C};\ X_4 = \frac{l_l}{l_g} = 1;\ X_5 = \frac{X_1 X_2^2 - 1}{4};\ X_6 = 1;$$

The coupled loss ratio obtained by the optimization of the loss function for different foot print area ratio is as shown in Table 1. The loss ratio between coupled to uncoupled converter circuits, is decreasing with the variation of foot print area (FPA) ratio. The maximum ratio is 91% at FPA ratio 0.6 and the minimum is 89% at FPA ratio equal to 1.5. Thus, there is an approximately 9% reduction in the total losses in the coupled system at FPA ratio equal to 0.6, and 11% reduction at FPA ratio equals to 1.5.

With these optimization results, design engineer can select suitable core dimensions for low loss and high efficiency. Fig. 8 shows the plot of optimization results showing the reduction in loss ratio with the variation of foot print area ratio.

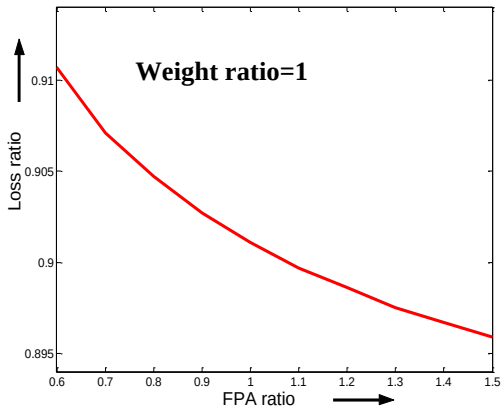


Fig. 8: Loss ratio reduction with variation of foot print area ratio

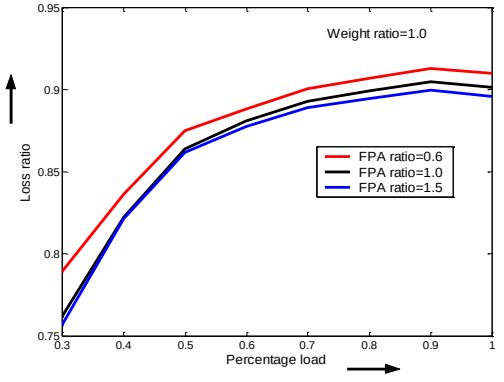


Fig. 9. Loss ratio variation with change in load for different FPA ratio.

Fig.9: shows the plot of loss ratio estimated against percentage loads for different foot print area ratio.

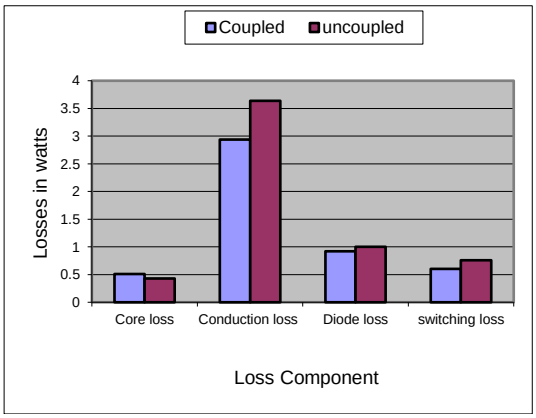


Fig. 10: Loss components in uncoupled and coupled converters

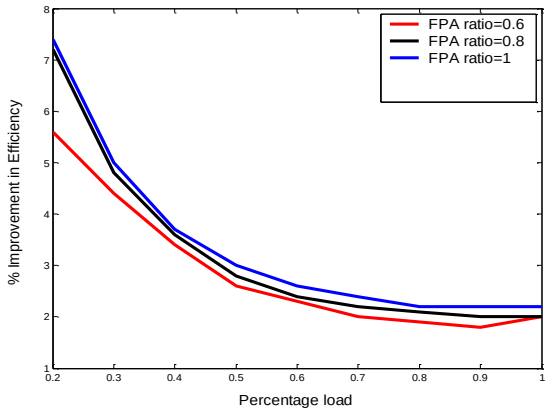


Fig. 11: Improvement in efficiency with variation of loads for different FPA ratio

From the plots it is clear that, for the entire load range the loss ratio is less than unity for small foot print area ratio. Thus, by using coupled inductor, double advantage of having less loss and less foot print area as compared to uncoupled multiphase buck converter can be achieved. Fig. 10 shows the loss components in uncoupled and coupled converters at full load.

Fig.11 shows the simulation plots of improvement in efficiency against percentage loads for different FPA ratio

Similarly, Fig. 12 shows the comparison of simulated and experimentally obtained loss ratios versus percentage loads at FPA ratio=1.

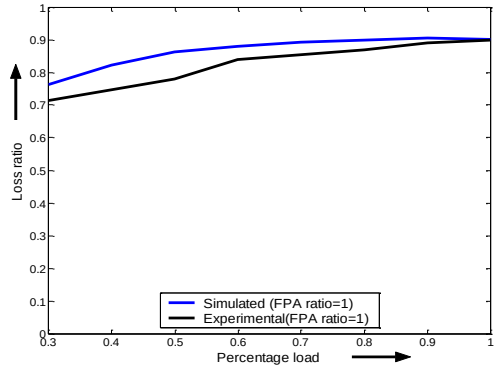


Fig. 12. Comparison of simulated and experimental results of loss ratio

Figure 13 shows the plot of Efficiency improvement in coupled system at different FPA ratios.

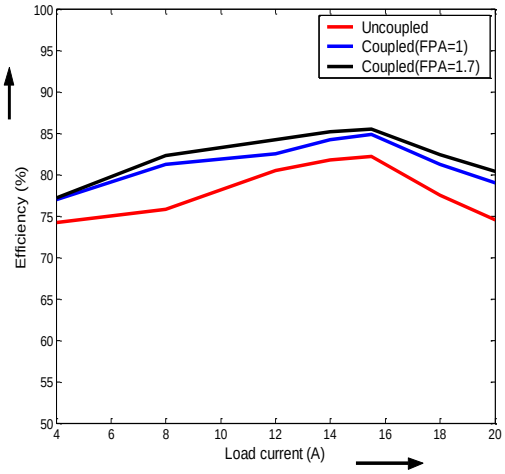


Fig. 13. Improvement in efficiency with variation of FPA ratio

## VI. Conclusion

In this paper, we have presented the design and optimization of the coupled core topology for a multiphase synchronous buck converter. It is shown that, by going for coupling, total losses can be minimized. A new core structure with common leakage path and air gap adjusts the Ampere-turn requirements and minimizes the phase ripples to a greater extent. Hence, by going for this type of structure and by selecting a high permeability material, a minimum of 10% loss reduction can be achieved. Thus, an overall efficiency of 2% to 4% can be predicted with this much loss reduction. However, by experiment, we have proved that, by using coupled inductor topology, 3-4% efficiency can be improved as compared to uncoupled converter system. As we can predict the efficiency with loss estimation technique, this approach helps the design engineer in selecting the material and the size of the core. Experimentally, it is also shown that the loss components in coupled converter are less as compared to uncoupled converter.

## VI. References

[1] Xunwei Zhou, Pit -leong Wong, Peng Xu, F. C. Lee, and Q. Huang, "Investigation of Candidate VRM topologies for future Microprocessors", IEEE Transactions on Power electronics, Vol. 15, no. 6, pp. 1172-82, 2000.

[2] W. Chen, Fred C. Lee, P. Xu. "Integrated Planar Inductor Scheme for Multi Module Interleaved QSW DC-DC Converter", IEEE PESC 1999, Vol. 2, pp. 759-762.

[3] Peng Xu, Jia wei, F. C. Lee, "A Active Clamp Couple Buck Converter - A Novel high efficiency VRM", IEEE APEC 2001, Vol. 1, pp.252-257.

[4] P.-L.Wong, Peng Xu, and Fred C. Lee, "Investigating coupling Inductors in the Interleaving QSW VRM", Proc. APEC 2000, vol. 2, pp. 973-78.

[5] P.-L.Wong, Peng Xu, P. Yang, and F. C. Lee, "Performance Improvements of Interleaving VRM with Coupled Inductors",IEEE Trans. Power Electronics, Vol. 16, no.4, pp. 499– 507, 2001.

[6] Jieli Li, Charles R. Sullivan and Aaron Schultz, "Coupled Inductor Design Optimization for fast Response Low Voltage DC - DC Converters", APEC 2002, vol. 2, pp. 817- 823.

[7] Jens Czogalla, Jieli Li, Charles R. Sullivan, "Automative Application of Multi-phase Coupled Inductor DC-DC Converter", IEEE Industry application society 2003, pp. 115-120.

[8] J. O'Connor, "Converter Optimization for Powering Low Voltage High Performance Microprocessors", Proc. IEEE APEC 1996, pp. 984-989.

[9] Y. Panov and M. M. Jovanovic, "Design Considerations for 12V / 1.5V, 50A Voltage Regulator Modules," Proc. IEEE APEC 2000, pp. 39-46.

[10] K. Yao, P.-Leong Wong and F. C. Lee, "The Inductor Design for the Multi-channel VRM," Proc. HFPC Conf., 2000, pp. 231-238.

[11] I. Jitaru and A. Ivascu, "Increasing the Utilization of the Transformers Magnetic Core by using Quasi-Integrated Magnetics," Proc. CPES Seminar, 2000, pp. 112-115.

[12] S.Cuk, "New Magnetic Structures for Switching Converters IEEE Trans. On Magnetics, March 1983, pp. 75- 83.

[13] H. N. Nagaraja, D. Kastha and Amit Patra, "Generalized Analysis of Integrated Magnetic Component based Low Voltage Interleaved DC-DC Buck Converter for Efficiency Improvement", Proc. IEEE ISCAS 2005, pp. 2485-2489.

[14] H. N. Nagaraj, D. Kastha and Amit Patra, "Design Optimization of Coupled Inductor Multiphase Synchronous Buck Converter," Proc. IEEE ICIT 2005, pp. 744-749.

[15] S. Cuk, L. Stevanovic and E. Santi, "Integrated Magnetic Design with Flat Low Profile Core," Proc. HFPC Conf. 1990.

[16] I. W. Hofsajar, J. D.Van Wyk and J. A.Ferreira, "Volume Considerations of Power Integrated Components," Proc. IEEE PESC, 1999, pp. 741-745.

[17] M. Rascon, R. Prieto, O. Garcia, J. A. Cobos and J. Uceda, "Design of Very Low Profile Magnetic Components using Flex Foils," Proc. IEEE APEC, 1997, pp. 561-567.

[18] S. Ramakrishnan, R. L. Steigerwald and J. A. Mallick, "A Comparison Study of Low Profile Power Magnetic for High Frequency High Density Switching Converters," Proc. IEEE APEC 1997, pp. 338-394.

[19] D. Y. Chen, "Comparison of High Frequency Magnetic Core Loss under two different conditions: A Sinusoidal Voltage and a Square Wave," Proc. IEEE PESC 1978, pp. 237-237-241

[20] N. Dai, W. Lofti, G. Skutt, W. Tabiz and F. C. Lee, "A Comparative Study of High Frequency Low- Profile Planar Transformer Technologies," Proc. IEEE PESC 1994, pp. 226-232.